Anthropocene 25 (2019) 100193

Contents lists available at ScienceDirect

Anthropocene

journal homepage: www.elsevier.com/locate/ancene

Impact of climate change on precipitation patterns in Houston, Texas, USA

Zhiying Li[a,*], Xiao Li[b], Yue Wang[b], Steven M. Quiring[a]

[a] Department of Geography, The Ohio State University, Columbus, OH, USA
[b] Department of Geography, Texas A&M University, College Station, TX, USA

ARTICLE INFO

Article history:
Received 26 October 2018
Received in revised form 25 January 2019
Accepted 30 January 2019
Available online 1 February 2019

Keywords:
Precipitation
Climate change
Indices
Clear Creek watershed

ABSTRACT

Extreme precipitation events damage infrastructure and property; thus, predicting future precipitation patterns in the context of climate change is important. In this study, precipitation projections from 36 downscaled General Circulation Models (GCMs) under two Representative Concentration Pathway (RCP) scenarios (RCP2.6 and RCP8.5) enabled examination of projected changes in future precipitation for the Clear Creek watershed in Houston, Texas, USA. Precipitation from 1950 to 2099 simulated with GCM were downscaled using the Bias-Correction Spatial Disaggregation method. Ten precipitation indices that represent precipitation amount, precipitation intensity, precipitation duration, and precipitation frequency evaluated how precipitation patterns will likely change. Results show that, at the annual scale, mean precipitation will significantly decrease based on RCP8.5, or remain relatively constant based on RCP2.6. Precipitation intensity and precipitation variability, however, will likely increase. Dry periods will lengthen significantly, whereas the length of wet spells will generally remain unchanged. At the monthly scale, the amount of precipitation, precipitation intensity, precipitation frequency and the length of wet spells will likely increase in September. In contrast, precipitation will likely decrease and dry spells will lengthen in April, May, August, November, and December. This finding illustrates that the intra-annual variability in precipitation will increase. The projected changes in precipitation under RCP8.5 are generally greater compared with RCP2.6. Differences between the scenarios are more pronounced towards the end of the century. Houston has recently experienced substantial precipitation variability, including severe drought and record-breaking precipitation from Hurricane Harvey in 2017. These events are consistent with the long-term GCM projections. Findings from this study can be applied to help manage water resources and enhance adaptability to climate change.

1. Introduction

Climate change directly influences precipitation and intensifies the global hydrological cycle (Trenberth, 2011). A warming climate will increase evaporation, leading to greater precipitation intensity because of the increased amount of water vapor in the atmosphere. These changes will increase the risk of extreme precipitation and flooding (Kundzewicz et al., 2014; Trenberth, 2011; Wasko and Sharma, 2017). Precipitation patterns are capturing more attention in scientific studies because extreme rainfall events can impact people substantially (Fowler and Kilsby, 2003; Rosenzweig et al., 2002; Westra et al., 2014). Improved understanding of precipitation patterns in the context of a changing environment will improve decision-making and lead to increased adaptive capacity in communities that experience extreme weather events.

In many regions around the world, precipitation patterns have changed in recent decades. These changes will likely continue into the future. Precipitation has increased since 1901 over mid-latitude land areas of the Northern Hemisphere (IPCC, 2013). Increases in the frequency and intensity of extreme precipitation events have occurred in North America and Europe (IPCC, 2013). Regional studies have also confirmed increasing trends in extreme precipitation events in the United States (USA) and other countries (Easterling et al., 2000). Although many studies have examined the relationships between precipitation patterns and climate change, the future impacts of climate change are still unclear because of the considerable uncertainty in General Circulation Model (GCM) simulations of precipitation (Rajczak and Schär, 2017; Woldemeskel et al., 2012; Zarekarizi et al., 2016).

Mean annual precipitation will likely increase in high latitudes and decrease in many mid-latitude and subtropical regions, under

* Corresponding author.
E-mail address: li.8254@osu.edu (Z. Li).

http://dx.doi.org/10.1016/j.ancene.2019.100193
2213-3054/

the Representative Concentration Pathway (RCP) 8.5 scenario (IPCC, 2013). At the regional scale, changes in precipitation patterns will vary by region. Gao et al. (2008) showed that future monsoon precipitation will likely decrease in China, for example, whereas Shields et al. (2016) demonstrated that the west coast of the USA will experience an increase in mean annual precipitation. Changes in extreme weather events will not be uniform across the globe (Beniston et al., 2007; Easterling et al., 2000; Kunkel, 2003). These variations call for an improved understanding of the trends of precipitation patterns at regional scales. Such an understanding is especially important since many regions may experience an increase in extreme precipitation events and flooding in the future.

This study focuses on Houston, Texas, USA because it has frequently experienced extreme rainfall events and flooding events in recent years. Home to about 2.3 million people (US Census, 2017), Houston is among the fastest growing cities in the state of Texas. Because of its low-lying geography, proximity to the Gulf of Mexico and unregulated urban development, flooding is a common problem in Houston. In August 2017, Hurricane Harvey caused extreme flooding in Houston and its surrounding areas. The flooding affected >100,000 homes and caused over 80 deaths (van Oldenborgh et al., 2017). Urban flooding causes severe impacts for people in terms of pollution, power outages. It can also disrupt lifeline systems like hospitals, nursing homes and water treatment facilities (Chang et al., 2007). Climate change will likely increase the annual probability of Houston receiving rainfall in excess of 500 mm by twenty-fold from 0.05% (once in 2,000-y) in 1981–2000 to 1% (once in 100-y) in 2081–2100 under RCP8.5 (Emanuel, 2017). Therefore, quantifying how other aspects of precipitation may change in Houston in the future is critical.

General Circulation Models (GCMs) simulate the historical and future climate under different greenhouse gas forcing scenarios. The spatial resolution of a GCM is too coarse, however, for regional studies. Therefore, downscaling techniques are necessary to improve the spatial resolution. This paper utilizes bias-correction spatial disaggregated (BCSD) multi-model ensembles from Coupled Model Intercomparison Project Phase 5 (CMIP5) to investigate the impact of climate change on precipitation patterns in the Clear Creek watershed in Houston, Texas under the RCP2.6 and RCP8.5 scenarios. This paper examines three research questions: (1) What are the projected future changes in annual precipitation patterns? (2) What are the projected future changes in monthly precipitation patterns? (3) How consistent are the projected changes in precipitation patterns between the two emissions scenarios? We hypothesize that in the future: (a) the number of extreme precipitation events will increase; (b) intra-annual variability of precipitation will increase; (c) the RCP8.5 scenario will have a larger impact on precipitation patterns. Results of this work have potential to facilitate evaluation of the resilience of flood control infrastructure, and improve water resources management and risk analysis.

2. Data and methods

2.1. Study area

The Clear Creek watershed (Fig. 1) encompasses portions of 19 cities, with Houston and Pearland comprising the largest proportion of the watershed (Table 1). This was determined by examining the watershed boundary obtained from the USGS (https://viewer.

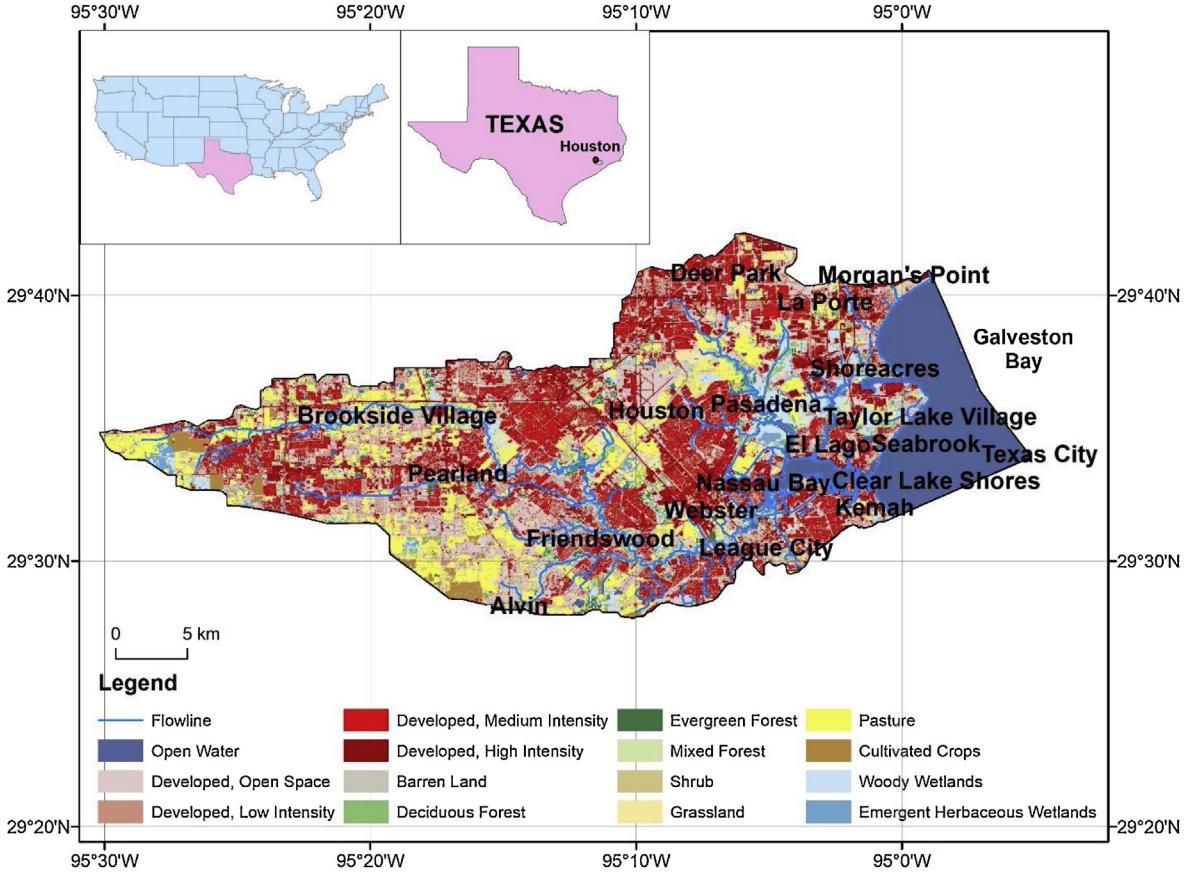

Fig. 1. Clear Creek Watershed in Houston, TX, USA. The top two maps show the geographic location of the watershed. The bottom map shows the watershed boundaries and the NLCD (2011) land use classification. The watershed is dominated by developed land and it contains 19 cities.

Table 1
List of the 19 cities within the Clear Creek watershed near Houston, TX. The first column represents the name of the cities and the second column represents the area of the city within the watershed. The city areas within the watershed are obtained by overlapping watershed boundary shapefile from the USGS (https://viewer.nationalmap.gov/basic/) and city boundary shapefile from the Texas Natural Resources Information System (https://tnris.org/data-catalog/entry/political-boundaries/).

City Name	Area of city within the watershed (km^2)
Houston	132.61
Pearland	114.05
League City	64.07
Pasadena	56.65
Friendswood	51.32
Seabrook	48.98
La Porte	36.16
Deer Park	17.17
Webster	17.08
Nassau Bay	5.98
Brookside Village	5.43
Kemah	3.66
Taylor Lake Village	3.63
Shoreacres	2.99
El Lago	1.85
Morgan's Point	1.65
Clear Lake Shores	1.49
Texas City	0.67
Alvin	0.64

nationalmap.gov/basic/) and the city boundaries obtained from the Texas Natural Resources Information System (https://tnris.org/data-catalog/entry/political-boundaries/). For convenience, we will describe this watershed as being located in Houston, because that is the city that comprises the largest proportion of the watershed. The study watershed has a drainage area of 771 km^2 (298 mi^2; Hydrologic Unit Code 1204020401) and comprises two primary streams that flow east into Galveston Bay. This region has urbanized significantly since the 1980s (Zhu et al., 2015). As calculated from the land use maps from National Land Cover Database, developed area increased from 27.40% in 1992 to 61.25% in 2011. Therefore, urbanization exacerbates flooding when it occurs, causing extensive property damage. The watershed has a wide floodplain and limited topographic relief. Given its proximity to the Gulf of Mexico, it is prone to extreme rainfall and flooding events, especially because of tropical cyclones (TCs). Tropical Storm Allison in 2001 and Hurricane Ike in 2008, for example, were responsible for >75% of the insured flood losses claimed during the period from 1999 to 2009 (Brody et al., 2018). Due to the combination of urbanization, geographic location and climate change, this area is vulnerable to extreme rainfall events.

2.2. CMIP5 multi-model ensemble

The multi-model, multi-scenario, bias-corrected and spatial disaggregated (BCSD) precipitation data were obtained from the World Climate Research Program's (WCRP's) Coupled Model Intercomparison Project Phase 5 (CMIP5; http://gdo-dcp.ucllnl.org/downscaled_cmip_projections). The multi-model ensemble utilized in this study includes daily precipitation data from 36 climate projections with 1/8-degree spatial resolution from 1950 to 2099. A total of 11 grid cells that overlap the watershed were extracted and combined using an area-weighted average to determine the precipitation for the watershed. Precipitation projections are not available for Dec 31, 2099 from one of the 36 models (bcc-csm1-1.1) in the RCP8.5 scenario. Therefore, calculation of the monthly and annual ensemble median does not include values of the bcc-csm1-1.1 model in December and in 2099 under RCP8.5. The multi-model ensemble is generally more reliable and consistent than individual model in estimating future climate conditions (Hagedorn et al., 2005; Weigel et al., 2008). Using ensemble median and percentiles is a common practice to reduce uncertainty in literature about multi-GCM projections (Dale et al., 2017; Gharbia et al., 2016; McSweeney and Jones, 2016). Therefore, the multi-model median values and the 10th and 90th percentiles for the precipitation indices were analyzed. Precipitation indices in three future time periods, 2010–2039, 2040–2069, and 2070–2099, representing near, mid-century, and end-of-century periods, were compared with indices from the baseline period (1950–1999). Precipitation patterns during the last 50 years in the 21st century (2050–2099) and in the 20th century (1950–1999) were also compared.

Observed monthly precipitation for the baseline period 1950–1999 were obtained from PRISM (Parameter-elevation Regression on Independent Slopes Model) AN81 m datasets (PRISM Climate Group, 2014) and were used to evaluate model performance. The PRISM data are quality-controlled observations from multiple monitoring networks. Many watershed-scale studies have used PRISM data (Daly et al., 2017; Grant et al., 2013; Strachan and Daly, 2017). The spatial resolution of the PRISM is 2.5 arcmin (~4 km).

2.3. Relative concentration pathways

The CMIP5 climate projections are based on the Representative Concentration Pathways (RCPs) from the Fifth Assessment Report of the Intergovernmental Panel on Climate Change (IPCC; IPCC, 2013). The report identified four RCPs (RCP2.6, RCP4.5, RCP6.0, and RCP8.5), each representing the approximate net radiative forcing ($W\ m^{-2}$) in 2100 relative to 1750. Different plausible ways in which future population growth, technological development and international policy may influence greenhouse gas emissions drive the scenarios. This study analyzed RCP2.6 and RCP8.5 because they represent the best-case (low emissions) and worst-case (high emissions) scenarios, respectively. The examination of these two scenarios provides an assessment of the range of potential changes in precipitation patterns in the study watershed.

2.4. Precipitation indices

The Expert Team on Climate Change Detection and Indices (ETCCDI) developed a set of 27 extreme climate indices. Many studies have used these indices to estimate historical and expected climate trends in different parts of the world (Alexander et al., 2006; Shrestha et al., 2017; Zarekarizi et al., 2016). A total of 10 precipitation indices quantifying precipitation amount, intensity, frequency, and duration were selected for this analysis (Table 2). This study analyzed projected changes in both annual and monthly precipitation. The total wet-day precipitation index (PRCPTOT) represents the precipitation amount on wet days (daily precipitation $\geq$ 1 mm). The five precipitation intensity indices that we are using are the very wet day index (R95pTOT), the extremely wet day index (R99pTOT), the maximum 1-day precipitation index (Rx1day), the maximum 5-day precipitation index (Rx5day), and the simple daily intensity index (SDII). The very wet day index (R95pTOT) and extremely wet day index (R99pTOT) indices represent precipitation on days where total precipitation is greater than the 95th percentile and the 99th percentile, respectively. The maximum 1-day precipitation index (Rx1day) and maximum 5-day precipitation index (Rx5day) represent the maximum amount of precipitation during a given month or year that falls on a single day and a consecutive 5-day period, respectively. The simple daily intensity index (SDII) is the total precipitation divided by the number of wet days in a given time period. This gives an average rainfall rate on each wet day. The number of heavy precipitation days (R10) and the number of very heavy precipitation days (R20) characterize the frequency of extreme rainfall, and represent the

Table 2
Description of the ten extreme precipitation indices defined by ETCCDI. The table provides a description of each index, the abbreviation used in this paper, how it is calculated and the unit of measurement. More details can be found at: http://www.climdex.org/indices.html.

Index	Abbreviation	Definition	Units
Amount			
Total wet day precipitation	PRCPTOT	Total precipitation on wet days (daily precipitation $\geq$ 1 mm)	mm
Intensity			
Precipitation on very wet days	R95pTOT	Total precipitation when daily precipitation >95th percentile	mm
Precipitation on extremely wet days	R99pTOT	Total precipitation when daily precipitation >99th percentile	mm
Max 1-day precipitation	Rx1day	Maximum 1-day precipitation	mm
Max 5-day precipitation	Rx5day	Maximum consecutive 5-day precipitation	mm
Simple daily intensity index	SDII	Total precipitation divided by the number of wet days (daily precipitation $\geq$ 1 mm)	mm day^{-1}
Frequency			
Number of heavy precipitation days	R10	Count of days when precipitation $\geq$ 10 mm	days
Number of very heavy precipitation days	R20	Count of days when precipitation $\geq$ 20 mm	days
Duration			
Consecutive wet days	CWD	Maximum number of consecutive days when daily precipitation $\geq$ 1 mm	days
Consecutive dry days	CDD	Maximum number of consecutive days when daily precipitation < 1 mm	days

number of days in a year or a month in which precipitation is no less than 10 mm and 20 mm, respectively. The consecutive wet day (CWD) index and the consecutive dry day (CDD) index are the two duration indices, and correspond to the maximum number of consecutive days with more than 1 mm of precipitation and with no more than 1 mm of precipitation, respectively. These two indices emphasize dry and wet spells in the area of interest. More information about ETCCDI is available at: http://etccdi.pacificclimate.org/list_27_indices.shtml.

2.5. Statistical analysis

The Mann-Kendall test is used in this study to evaluate the significance of the trends in the monthly and annual precipitation indices from 1950 to 2099. Friedman's test is used to evaluate the significance of the differences in the precipitation indices index between the two scenarios. The Friedman's test is a non-parametric statistical test for an experimental design involving two factors (Hollander et al., 2013). The goal is to test the location effects (medians) of the treatment factor within the different levels of the blocking factor (Hollander et al., 2013). The blocking factor is treated as homogeneous subgroups of subjects (Hollander et al., 2013). In this case, the treatment factors are the RCP2.6 and RCP8.5 scenarios and the blocking factor is time.

3. Results

3.1. Comparison with gridded observed data

This study first investigates how well the ensemble median and the model spread reproduce the observed precipitation in the baseline period. At the annual scale (Fig. 2a), the spread of models is able to capture the observed precipitation, although the ensemble median does not agree with the observed data in all years. The ensemble median tends to overestimate annual precipitation during dry periods (e.g. the 1950s) and underestimate it during wet periods (e.g. the 1970s and the 1990s). In addition, the ensemble median underestimates the inter-annual variability of observed precipitation. Overall, the 50-year average (1950–1999) of the ensemble median is lower than the observed data by 4.97%. This relatively small difference suggests that the ensemble median is able to simulate the observed values well over longer time periods.

As seen from the monthly precipitation in 1950–1999 (Fig. 2b), the observed data fall within the model spread, except in June, August, and November, when the observed data are slightly higher than the maximum value of the modeled data. The ensemble median matches the observed data best in February, when the relative difference between modeled and observed

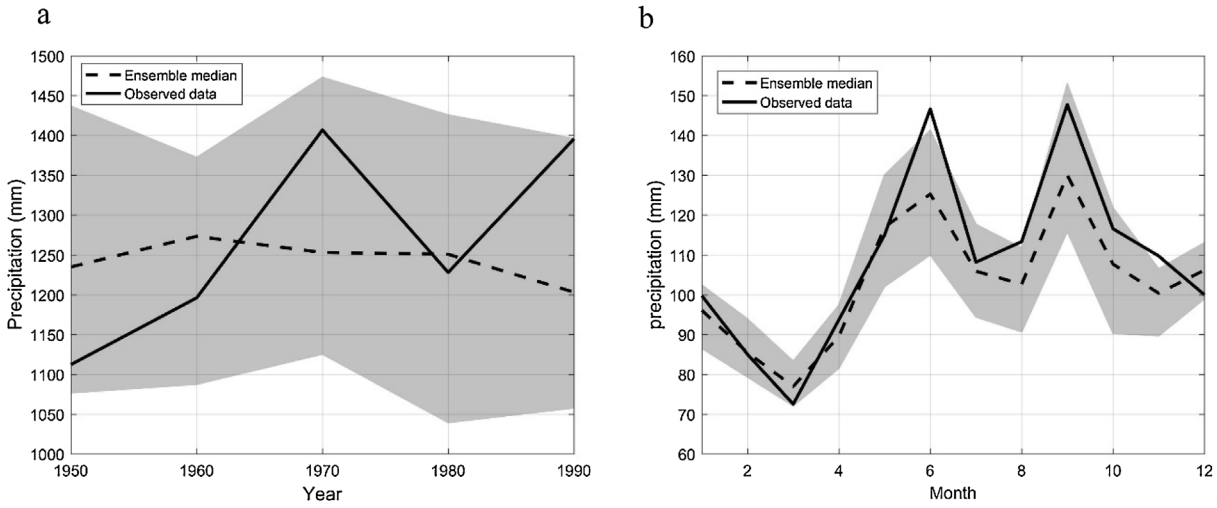

Fig. 2. Comparison between CMIP5 modeled and observed PRISM precipitation in the Clear Creek Watershed (Houston, TX) from 1950 to 1999 at (a) annual scale and (b) monthly scale. Data at annual scale are decadal average values for five 10-year periods. The shaded areas represent the range based on the maximum and minimum values from individual models. The dash lines are the multi-model ensemble median. The solid lines are the observed data.

precipitation is 0.54%. Similar to the annual pattern, the ensemble median underestimates the wetter months (e.g. in June by −14.57% and September by −11.99%) and overestimates the drier months (e.g. in March by 6.10%). Thus, the underestimation of ensemble median at annual timescale during 1950–1999 mostly comes from the underestimation in June and September. Nevertheless, the ensemble median captures the seasonal cycle of precipitation quite well. The model-predicted maxima (June and September) and minima (March) agree with the observed data. On average, the monthly model predictions underestimate the observed data by 3.99%. Overall, the ensemble median provides a good representation of the observations over longer time-scales and the models can capture the seasonal cycle of precipitation.

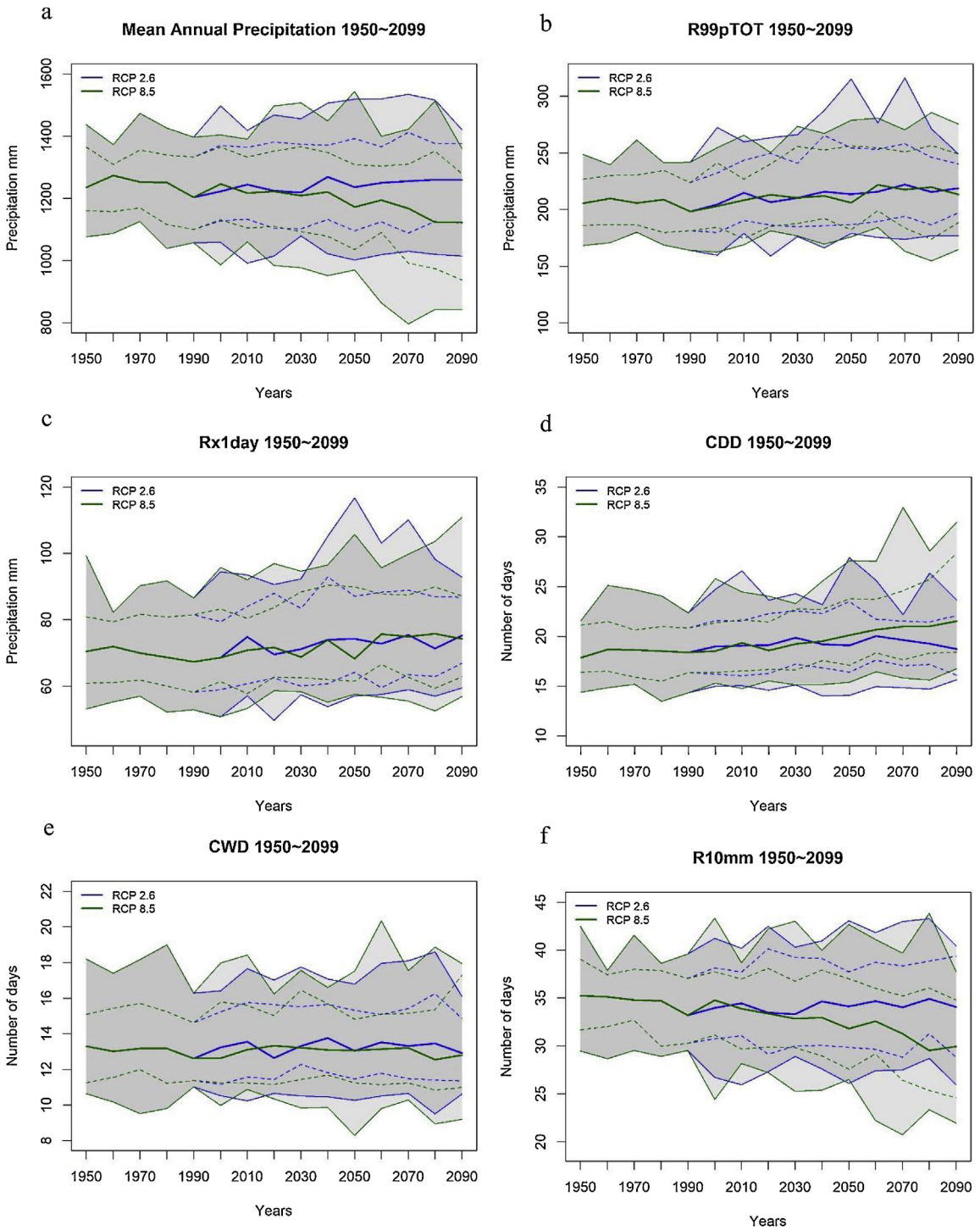

Fig. 3. CMIP5-simulated precipitation indices from 1950 to 2099 in the Clear Creek Watershed based on the RCP2.6 and RCP8.5 emissions scenarios: (a) mean annual precipitation (mm), (b) R99pTOT (%), (c) Rx1day (mm), (d) CDD (days), (e) CWD (days), and (f) R10 mm (days). All of the precipitation indices are described in Table 1. The bold solid green line represents the ensemble median for RCP8.5 and the bold solid blue line represents the ensemble median for RCP2.6. The dash lines represent the 10th and 90th percentiles and the solid lines delineating the shaded area represent the minimum and maximum values of the CMIP5 models. Data are decadal average values.

3.2. Annual precipitation indices

This study calculated annual precipitation indices from 1950 to 2099 and then calculated mean decadal values for each index for the RCP2.6 and RCP8.5 scenarios. Based on these data, mean annual precipitation remains relatively constant between 1950 and 2099 in RCP2.6. There is a slight increasing trend of 0.9 mm/decade (Fig. 3a; Table 3). In contrast, mean annual precipitation has a statistically significant decreasing trend of −8.9 mm/decade in RCP8.5 (Fig. 3a; Table 3). The wettest decade, in terms of mean annual precipitation for both RCP2.6 and RCP8.5, occurs in the 1960s. The changes in the mean annual precipitation in the last 50 years of the 21st century (2050–2099) with respect to the last 50 years of the 20th (1950–1999) century, range from −323.7 mm to 121.3 mm with a median of −61.2 mm for RCP8.5.

There are some decadal variations in the projected trends in mean annual precipitation. For RCP2.6, mean annual precipitation will likely decrease by 1.9 mm (−0.15%) in the near-term (2010–2039), increase by 13.7 mm (1.10%) by mid-century (2040–2069), and increase by 12.2 mm (0.98%) by the end-of-century (2070–2099). While RCP8.5 projects that mean annual precipitation will decrease in the near-term (−12.1 mm; −0.97%), mid-century (−43.0 mm; −3.46%), and the end-of-century period (−94.2 mm; −7.58%) with respect to 1950–1999 (Table 4; Fig. 4).

Precipitation intensity will likely increase significantly by 2099 (Table 3). For example, the extremely wet day index (R99pTOT) will likely increase in both emissions scenarios (Fig. 3b). Specifically, compared with the baseline period (1950–1999), the median R99pTOT will increase by 5.3 mm (2.58%), 9.7 mm (4.67%) and 13.2 mm (6.39%) in the near-term (2010–2039), mid-century (2040–2069), and end-of-century (2070–2099) periods for the RCP2.6 scenario. In the RCP8.5 scenario, R99pTOT will increase by 5.9 mm (2.89%), 7.6 mm (3.67%), and 12.7 mm (6.13%) in the corresponding periods (Table 4; Fig. 4). The increase in precipitation intensity is generally most pronounced by the end of the century.

Another indication of increasing precipitation intensity is shown by Rx1day (Fig. 3c). There is a statistically significant increase in Rx1day of 0.4 mm/decade for both emissions scenarios (Table 3). Like R99pTOT, the increases are greatest towards the end of the century, with a median increase of 4.0 mm (5.69%) for RCP2.6 and 5.7 mm (8.02%) for RCP8.5 (Table 4; Fig. 4). The pattern of changes in Rx5day is similar to Rx1day, but it shows even larger relative changes than Rx1day by the end-of-century future. The simple daily intensity index (SDII) and R95pTOT also increase steadily in both the RCP2.6 and RCP8.5 scenarios (Table 3).

There is also a clear increase in the number of consecutive dry days (CDD) in the future (Fig. 3d), while the number of consecutive wet days (CWD) will likely remain relatively constant (Fig. 3e). There is a statistically significant increase in CDD of 0.09 days/decade for RCP2.6, and 0.24 days/decade for RCP8.5 (Table 3). The median increases in CDD are 0.54 days (2.90%), 0.73 days (3.93%), and 0.74 days (3.97%) for the near (2010–2039), mid-century (2040–2069), and end-of-century (2070–2099) periods with respect to 1950–1999 for RCP2.6. The median increase in CDD is more pronounced for RCP8.5, where it is 0.68 days (3.64%), 1.60 days (8.57%), and 2.62 days (13.99%) for the corresponding three periods. In contrast, CWD will only change modestly. It has an insignificant increase of 0.02 days/decade for RCP2.6 and an insignificant decrease rate of -0.01 days/decade for RCP8.5 (Table 3; Fig. 3e).

Precipitation frequency will generally decrease. There is a statistically significant decrease in R10 of -0.36 days/decade in RCP8.5 (Table 3; Fig. 3f), but the trend in RCP2.6 is not statistically significant. Specifically, R10 decreases by 0.98 days (−2.84%), 1.98 (−5.72%), and 3.75 days (−10.85%) in RCP8.5 in the near-term, mid-century and end-of-century, respectively (Table 4, Fig. 4). The maximum R10 values for both scenarios occur in the 1950s, while the minimum values occur in the 2080s for RCP8.5. There is also a statistically significant decreasing trend in R20 of -0.1 days/decade based on RCP8.5 (Table 3).

Apart from the changes in median, it is worth noting the spread amongst the models. The inter-model differences are quite large, which indicates uncertainty in the estimates from individual models (Fig. 3). The inter-model differences are larger towards the end of century, especially for RCP8.5. For example, the range of the 10th and 90th quantiles of mean annual precipitation for RCP8.5 in 2070–2099 is 345.5 mm, which is 146.1 mm larger than the range

Table 3
Trends in monthly and annual precipitation indices from 1950 to 2099 for RCP2.6 and RCP8.5 based on all CMIP5 models.

Scenario	Indices	Jan	Feb	Mar	Apr	May	Jun	Jul	Aug	Sep	Oct	Nov	Dec	Annual
RCP2.6	Precipitation amount (mm/decade)	−0.11	0.04	0.04	−0.41*	−0.46	0.06	−0.04	−0.17	1.81**	−0.12	−0.65*	−0.43*	0.94
	PRCPTOT (mm/decade)	−0.12	0.03	0.04	−0.42*	−0.46	0.09	−0.04	−0.16	1.82**	−0.10	−0.66*	−0.42*	1.07
	R95pTOT (mm/decade)	0.25*	0.16*	0.05	−0.23*	−0.30	0.11	−0.06	−0.11	1.49**	0.08	−0.30	−0.19	1.82**
	R99pTOT (mm/decade)	0.33**	0.03	0.07	−0.20*	−0.28*	0.00	−0.01	−0.04	0.81**	−0.09	−0.09	−0.07	1.07**
	Rx1day (mm/decade)	0.14*	0.09	0.05	−0.10	−0.02	0.07	0.00	−0.08	0.39*	0.03	0.01	−0.06	0.36*
	Rx5day (mm/decade)	0.16	0.04	0.07	−0.16	−0.06	0.22*	−0.04	−0.09	1.02**	0.08	−0.03	−0.07	1.28**
	SDII (mm/decade)	0.06**	0.01*	0.02	−0.03*	0.01	0.02	0.00	−0.01	0.08**	0.04*	0.00	0.00	0.02**
	CDD (days/decade)	0.03*	0.02	0.00	0.01	0.03*	0.01	0.00	0.00	−0.04**	0.02	0.09**	0.03**	0.08**
	CWD (days/decade)	−0.03*	−0.02*	0.00	−0.01	−0.02*	0.00	−0.02	0.00	0.04**	−0.02*	−0.02**	−0.02**	0.02
	R10 (days/decade)	0.00	0.00	0.00	−0.01	−0.02*	−0.01	0.00	−0.01	0.04**	0.00	−0.03*	−0.02**	−0.04
	R20 (days/decade)	0.00	0.00	0.00	−0.01*	−0.01	0.00	0.00	0.00	0.03**	0.00	−0.01	−0.01	0.04*
RCP8.5	Precipitation amount (mm/decade)	−0.92**	−1.02**	−1.24**	−1.29**	−1.82**	−1.23*	−0.97**	−1.07**	2.65**	−0.25	−1.44**	−1.42**	−8.87**
	PRCPTOT (mm/decade)	−0.94**	−1.03**	−1.24**	−1.28**	−1.83**	−1.23*	−0.98**	−1.09**	2.70**	−0.24	−1.42**	−1.42**	−8.79**
	R95pTOT (mm/decade)	−0.09	−0.20	−0.41	−0.77**	−0.88**	−0.18	−0.19	−0.33*	2.54**	0.26	−0.37	−0.46**	0.26
	R99pTOT (mm/decade)	0.19*	−0.03	−0.15	−0.31*	−0.28*	−0.17	−0.13	−0.14	1.27**	−0.07	0.10	−0.10	0.95**
	Rx1day (mm/decade)	−0.03	−0.15	−0.20*	−0.32**	−0.30**	−0.16	−0.12	−0.20**	0.60**	−0.07	−0.02	−0.17**	0.40*
	Rx5day (mm/decade)	−0.21	−0.37**	−0.42*	−0.63**	−0.68**	−0.42	−0.33	−0.47**	1.60**	0.17	−0.20	−0.37**	1.37**
	SDII (mm/decade)	0.02	−0.02	0.00	−0.02	−0.03	0.02	−0.03*	−0.04**	0.11**	0.06	0.06	0.01	0.01
	CDD (days/decade)	0.09**	0.08**	0.07**	0.08**	0.10**	0.11**	0.05**	0.05**	−0.05**	0.03*	0.16**	0.10**	0.24**
	CWD (days/decade)	−0.05**	−0.04**	−0.03**	−0.04**	−0.06**	−0.04**	−0.07**	−0.06**	0.08**	−0.02	−0.05**	−0.06**	−0.01
	R10 (days/decade)	−0.04**	−0.04**	−0.04**	−0.05**	−0.08**	−0.06**	−0.04**	−0.04**	0.06**	−0.02*	−0.06**	−0.05**	−0.36**
	R20 (days/decade)	−0.01*	−0.02**	−0.02**	−0.03**	−0.04**	−0.02*	−0.01	−0.01**	0.04**	0.00	−0.02*	−0.02**	−0.10**

* Significant at .05 level.
** Significant at .01 level.

Table 4
Median absolute changes and relative changes (%) in the annual precipitation indices in 2010–2039, 2040-69 and 2070–2099 with respect to 1950–1999 for RCP2.6 and RCP8.5 based on all CMIP5 models.

Indices	2010-2039		2040-2069		2070-2099	
	RCP2.6	RCP8.5	RCP2.6	RCP8.5	RCP2.6	RCP8.5
Mean annual precipitation (mm)	−1.92 (-0.15%)	−12.11 (-0.97%)	13.67 (1.10%)	−42.97 (-3.46%)	12.22 (0.98%)	−94.20 (-7.58%)
PRCPTOT (mm)	−1.57 (-0.13%)	−12.36 (-1.03%)	13.56 (1.13%)	−43.30 (-3.61%)	11.12 (0.93%)	−95.24 (-7.94%)
R95pTOT (mm)	8.67 (1.55%)	7.26 (1.30%)	23.79 (4.26%)	3.69 (0.66%)	22.25 (3.99%)	−1.02 (-0.18%)
R99pTOT (mm)	5.34 (2.58%)	5.98 (2.89%)	9.65 (4.67%)	7.59 (3.67%)	13.22 (6.39%)	12.68 (6.13%)
Rx1day (mm)	3.05 (4.31%)	1.65 (2.33%)	3.93 (5.55%)	4.48 (6.33%)	4.03 (5.69%)	5.68 (8.02%)
Rx5day (mm)	9.50 (6.78%)	12.48 (8.90%)	17.84 (12.73%)	12.82 (9.14%)	14.63 (10.44%)	18.64 (13.30%)
SDII (mm)	0.12 (1.59%)	0.07 (0.91%)	0.33 (4.26%)	0.12 (1.58%)	0.30 (3.88%)	0.02 (0.24%)
CDD (day)	0.54 (2.90%)	0.68 (3.64%)	0.73 (3.93%)	1.60 (8.57%)	0.74 (3.97%)	2.62 (13.99%)
CWD (day)	0.05 (0.35%)	−0.08 (-0.62%)	0.36 (2.75%)	0.23 (1.79%)	0.25 (1.92%)	0.03 (0.22%)
R10 (day)	−0.27 (-0.78%)	−0.98 (-2.84%)	−0.53 (-1.54%)	−1.98 (-5.72%)	0.24 (0.68%)	−3.75 (-10.85%)
R20 (day)	0.12 (0.86%)	−0.21 (-1.57%)	0.25 (1.81%)	−0.48 (-3.48%)	0.43 (3.14%)	−1.36 (-9.90%)

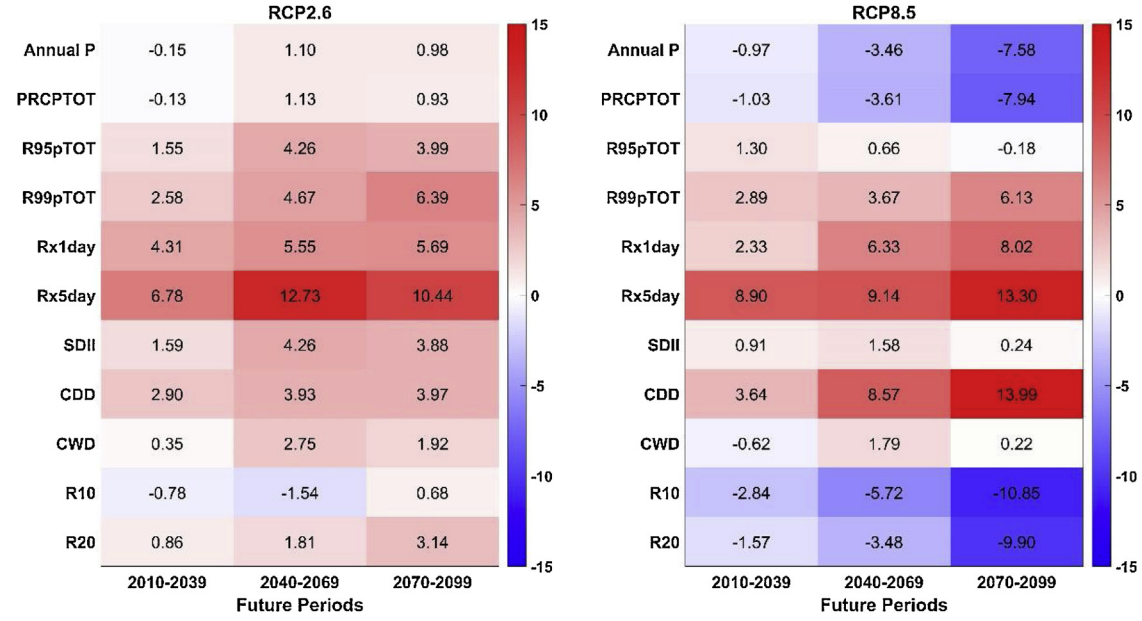

Fig. 4. Annual relative changes (%) in annual precipitation and the ten precipitation indices in 2010–2039, 2040-69 and 2070–2099 with respect to 1950–1999 for RCP2.6 and RCP8.5. Colors indicate the direction of change, with red (blue) colors representing increases (decreases). Darker colors represent larger magnitudes of change. Specific values of relative change (%) are labeled in each block.

in 1950–1999. Nevertheless, there is substantial overlap between the interquartile ranges of the two scenarios. This provides information about the most likely range in the future. The 10th and 90th percentiles of the modeled indices reflect the potential extreme cases. The 10th percentiles of the mean annual precipitation show a large decrease and the 90th percentiles of the CDD increase obviously under RCP8.5 scenario, indicating a substantial drying trend. As for precipitation intensity, the 90th percentiles of R99pTOT for RCP8.5 have an increasing rate of 2.3 mm/decade, which is larger than the trend of ensemble median (0.95 mm/decade; Table 3); while the 10th percentiles have a much smaller trend of only 0.12 mm/decade. This indicates that some models are predicting substantial increases in the intensity of very heavy rainfall. As for precipitation frequency, the 10th percentiles of the R10 mm for RCP8.5 have a substantial decreasing trend of -0.5 days/decade. Considering the extreme cases, it is possible that there will be many fewer precipitation events, but when it rains, it will be concentrated in short periods with very high intensity.

Overall, while there will be less precipitation in the future, precipitation intensity will increase significantly. The increases in precipitation intensity are greatest for the most extreme events (e.g., daily precipitation >99th percentile). Consecutive dry days will also significantly increase and dry spells will lengthen in the future. This indicates that conditions in the study watershed will shift to a more extreme hydrologic regime. More intense rainfall, leading to greater flooding risk, while, at the same time, the likelihood of longer dry spells and associated drought conditions will also increase. These changes in the hydrological cycle, will influence the frequency and intensity of droughts and floods and will subsequently increase the risk to property and human life in the urbanized areas of this watershed. A key takeaway from the annual analysis of is that, precipitation will decrease, but precipitation events will be larger and periods with little-to-no rain will lengthen.

3.3. Monthly precipitation indices

This study also examined the intra-annual changes in precipitation patterns in the Clear Creek watershed. September is the wettest month during the baseline period (1950–1999), followed by June. Therefore, precipitation in the study watershed has double maxima (Fig. 5). Mean monthly precipitation is lowest in March, then it increases until June and then declines until August, peaks in September and then decreases again. For near-

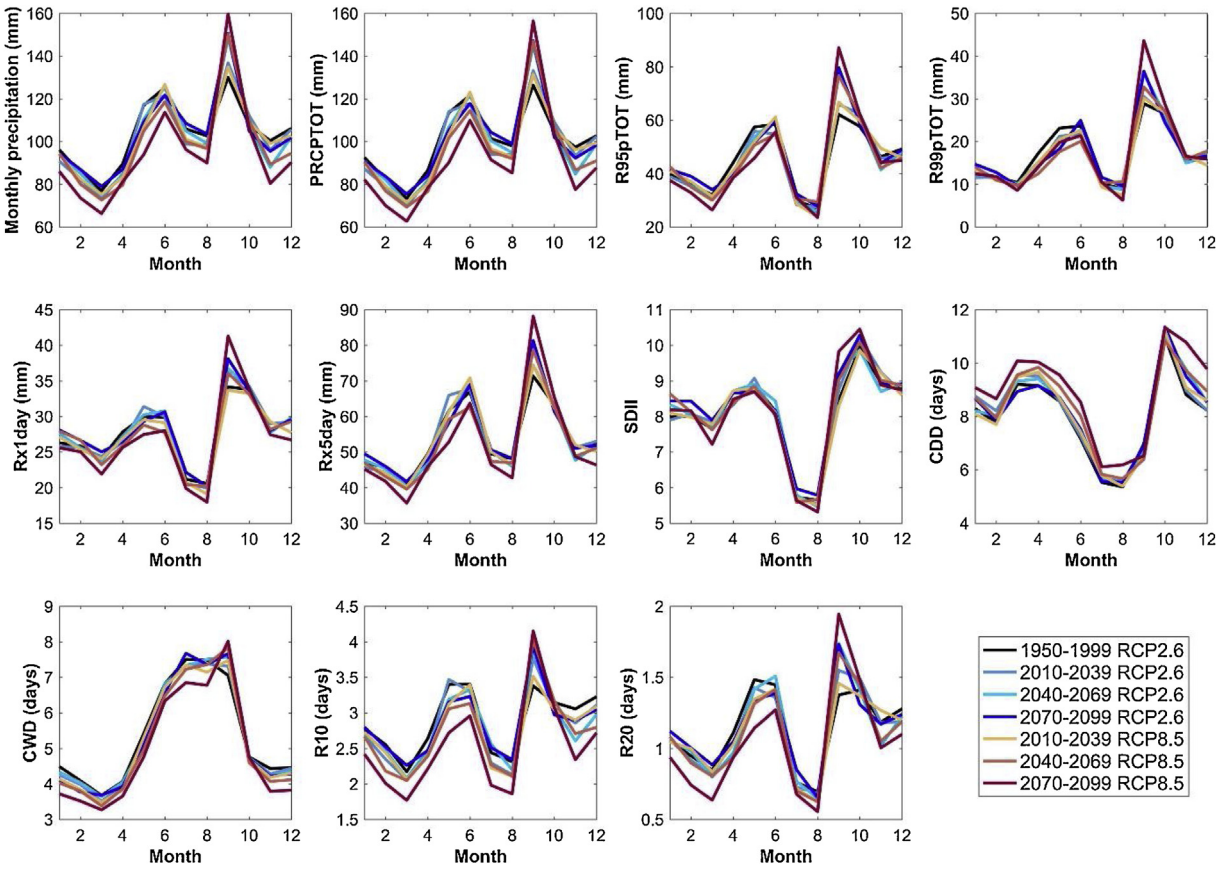

Fig. 5. Mean monthly precipitation (mm) and the ten monthly precipitation indices in 2010–2039, 2040-69 and 2070–2099 with respect to 1950–1999 for RCP2.6 and RCP8.5. The values reported here are the ensemble medians based on all of the CMIP5 models.

term, mid-century, and end-of-century periods for both emissions scenarios, the timing of the wettest and the driest months remains the same as during the baseline period.

The multi-model median monthly precipitation for RCP2.6 shows large increase in June and September, and shows large decreases in April, May, November and December. This indicates that the wettest months get wetter and the driest months get drier. Specifically, precipitation in September has the largest (statistically significant) increasing trend of 1.8 mm/decade and precipitation in November has the largest (statistically significant) decreasing trend of -0.6 mm/decade (Table 3). In contrast, RCP8.5 shows a decreasing trend in monthly precipitation for all months, except September. May is the month with the largest (statistically significant) decreasing trend of −1.8 mm/decade and September has a statistically significant increasing trend of 2.7 mm/decade (Table 3). Generally, the greatest changes in monthly precipitation occur towards the end of century.

The rainfall intensity indices increase significantly in September, and decrease significantly in April for both emissions scenarios. For example, September R95pTOT will increase at a rate of 1.5 mm/decade for RCP2.6 and 2.5 mm/decade for RCP8.5, while April R95pTOT will decrease significantly at a rate of -0.2 mm/decade for RCP2.6 and -0.8 mm/decade for RCP8.5 (Table 3). Rainfall intensity indices follow the double maxima pattern, with one peak occurring in September and another occurring in May or June (Fig. 5). These patterns will likely remain unchanged in future. With respect to baseline period, precipitation intensity in September will increase more than any other month. For example, the median September R95pTOT increases by 3.8 mm (6.06%) in the near-term (2010–2039), 16.1 mm (25.83%) in the mid-century (2040–2069), and 17.5 mm (28.09%) in the end-of-century (2070–2099) for RCP2.6; for RCP8.5, the median September R95pTOT increases by 4.5 mm (7.32%), 14.6 mm (23.53%), and 24.96 mm (40.16%) in the same three periods with respect to 1950–1999 (Fig. 6).

The rainfall intensity indices decrease significantly in a number of months, although the months with the largest decreases depend on the emissions scenario. In RCP2.6, R95pTOT decreases the most in April (-8.57%), November (−10.63%) and May (−10.20%) with respect to baseline period (Fig. 6). While in RCP8.5, R95pTOT decreases the most in May with declines of -5.6 mm (−9.80%), −6.8 mm (−11.90%) and −11.7 mm (−20.32%) in the three periods (Fig. 6).

Precipitation frequency follows a similar pattern to monthly precipitation amounts. The precipitation frequency will likely increase in months that are going to get wetter (September) and decrease in months that are going to get drier (April, May, November, and December). For example, there is a statistically significant increase in R10 in September of 0.04 days/decade for RCP2.6 and 0.06 days/decade for RCP8.5. There is a statistically significant decrease in R10 in May of −0.02 days/decade for RCP2.6 and -0.08 days/decade for RCP8.5 (Table 3). As for changes in three future periods, R10 in September has the largest median increase of 0.4 days (11.51%) in the near future, 0.5 days in the mid-century future (14.84%), and 0.6 days (16.94%) in the end-of-century future for RCP2.6 and of 0.1 days (4.1%), 0.6 days (19.0%) and 0.8 days (22.9%) for RCP8.5, with respect to 1950–1999 (Fig. 6). Months that have largest decreases in R10 are February in 2010–2039, November in 2040–2069, and May in 2070–2099 for RCP2.6 and May, December, and November in the corresponding periods for RCP8.5.

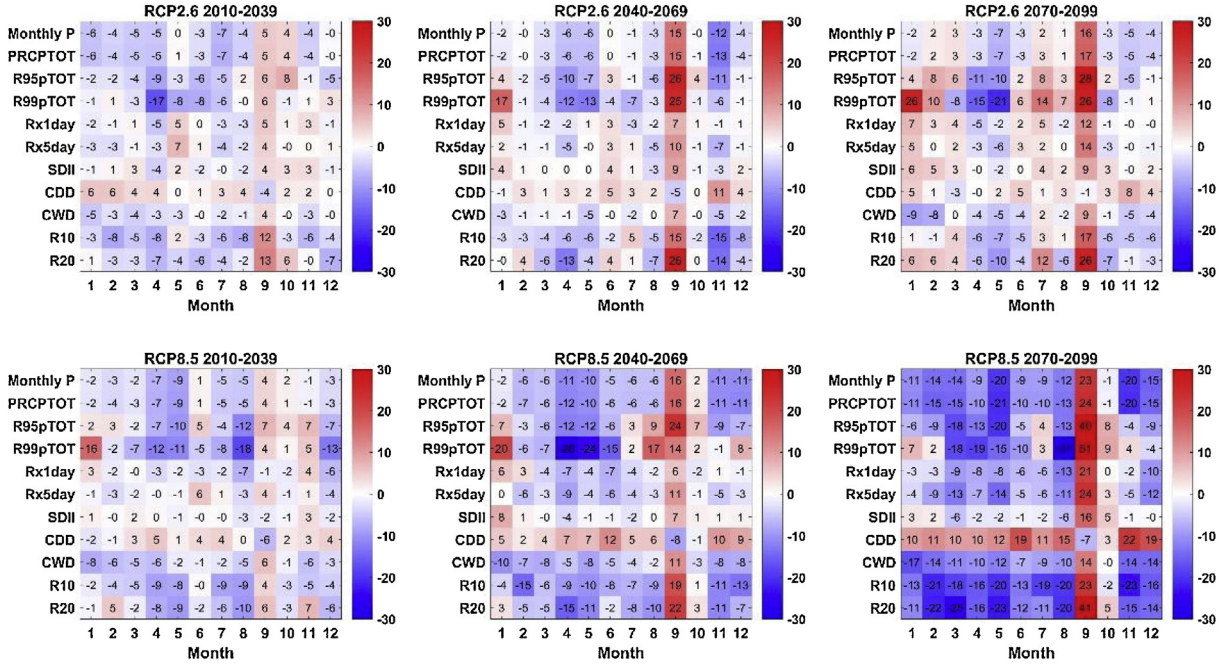

Fig. 6. Monthly relative changes (%) in monthly precipitation and the ten precipitation indices in 2010–2039, 2040-69, and 2070–2099 with respect to 1950–1999 for RCP2.6 and RCP8.5. The top row shows the results for RCP2.6 in 2010–2039, 2040-69 and 2070–2099. The bottom row shows the results for RCP8.5 in 2010–2039, 2040-69 and 2070–2099. Colors indicate the direction of change, with red (blue) colors representing increases (decreases). Darker colors represent larger magnitudes of change. Specific values of relative change (%) are labeled in each block.

CWD increases significantly only in September, and decreases in the remaining eleven months for both scenarios. The largest statistically significant decreasing trend occurs in January for RCP2.6 (-0.03 days/decade) and in July for RCP8.5 (-0.07 days/decade; Table 3). January usually has the largest decreases in future periods. By the end-of-century, for example, CWD will decrease in January by 0.4 days for RCP2.6 and 0.8 days for RCP8.5, with respect to baseline period (Fig. 6). September has the largest increases, with 0.6 days for RCP2.6 and 1.0 days for RCP8.5 by the end-of-century. There is only one CWD maximum throughout a year, which occurs in July during the baseline period, and it is predicted to shift to August or September in the future (Fig. 5). March is consistently the month with the lowest CWD in both the baseline and the future periods.

CDD shows pronounced increases in all months, except September, and in both emissions scenarios. The largest statistically significant increases occur in November in both scenarios (Table 3). November usually has the largest increasing number of CDD in all future periods. For example, CDD increases the most in November by 0.9 days (10.69%) for RCP2.6 and by 0.9 days (10.34%) for RCP8.5 in 2040–2069, with respect to 1950–1999 (Fig. 6). The only month that decreases significantly in CDD is September. There is a double maxima pattern of CDD, with one peak occurring in October or November and another in March or April (Fig. 5). July or August is always when CDD is at a minimum.

Apart from the analysis of the changes in ensemble median, the model spread can also give some insights into the extreme cases. This analysis focuses on September because September is the wettest month and has the highest values for most of the extreme indices. As seen from Fig. 7a, the 90th percentiles of September precipitation for both RCP2.6 and RCP8.5 increase from the 1950s to the 2090s, and the 10th percentiles remain relatively unchanged. This indicates a trend towards increased precipitation in September towards the end of century. Similarly, Fig. 7b indicates that the 90th percentile of R99pTOT has an increasing rate of 1.13 mm/decade for RCP2.6 and of 2.30 mm/decade for RCP8.5, while the 10th percentiles remain relatively unchanged. This suggests that some models tend to estimate a very high rainfall intensity at the end of the century. As for rainfall duration (Fig. 7d–e) and frequency (Fig. 7f), the percentiles of CDD in September do not show a substantial change from 1950 to 2099. In contrast, the 90th percentile of CWD for RCP8.5 has an increasing trend of 0.22 days/decade and the 90th percentile of R10mm for RCP8.5 has a trend of 0.17 days/decade. Another striking feature is that the 90th percentiles fluctuate substantially throughout the study period, especially for R99pTOT and Rx1day (Fig. 7b–c). Additionally, the range between the 10th and 90th percentiles increase from the 1950s to the 2090s, especially for RCP8.5. For example, September precipitation increases from 64.94 mm in the 1950s to 79.32 mm for RCP2.6 and to 149.71 mm for RCP8.5 in the 2090s. The increasing interquartile range indicates that there are relatively large differences between the models. This paper focuses on the ensemble median to analyze potential future trends, while acknowledging that considerable uncertainty exists.

Examination of the monthly variations in precipitation indices provides insights into the seasonal cycle of precipitation and allows for identifying contrasting patterns during difference months that may be obscured at the annual scale. For example, CDD is consistently decreasing in all months, except September. September is also the month that shows the greatest increases in precipitation and extreme precipitation.

3.4. Differences between emissions scenarios: RCP2.6 versus RCP8.5

There are similarities and differences between RCP2.6 and RCP8.5. Therefore, it is important to compare the results from these two emissions scenarios to determine what changes will likely occur in precipitation patterns in the Clear Creek watershed regardless of which emissions pathway followed in the future. The direction of change, for example, is relatively consistent between the two scenarios for most indices in most future periods. The primary difference between them is the magnitude of the changes.

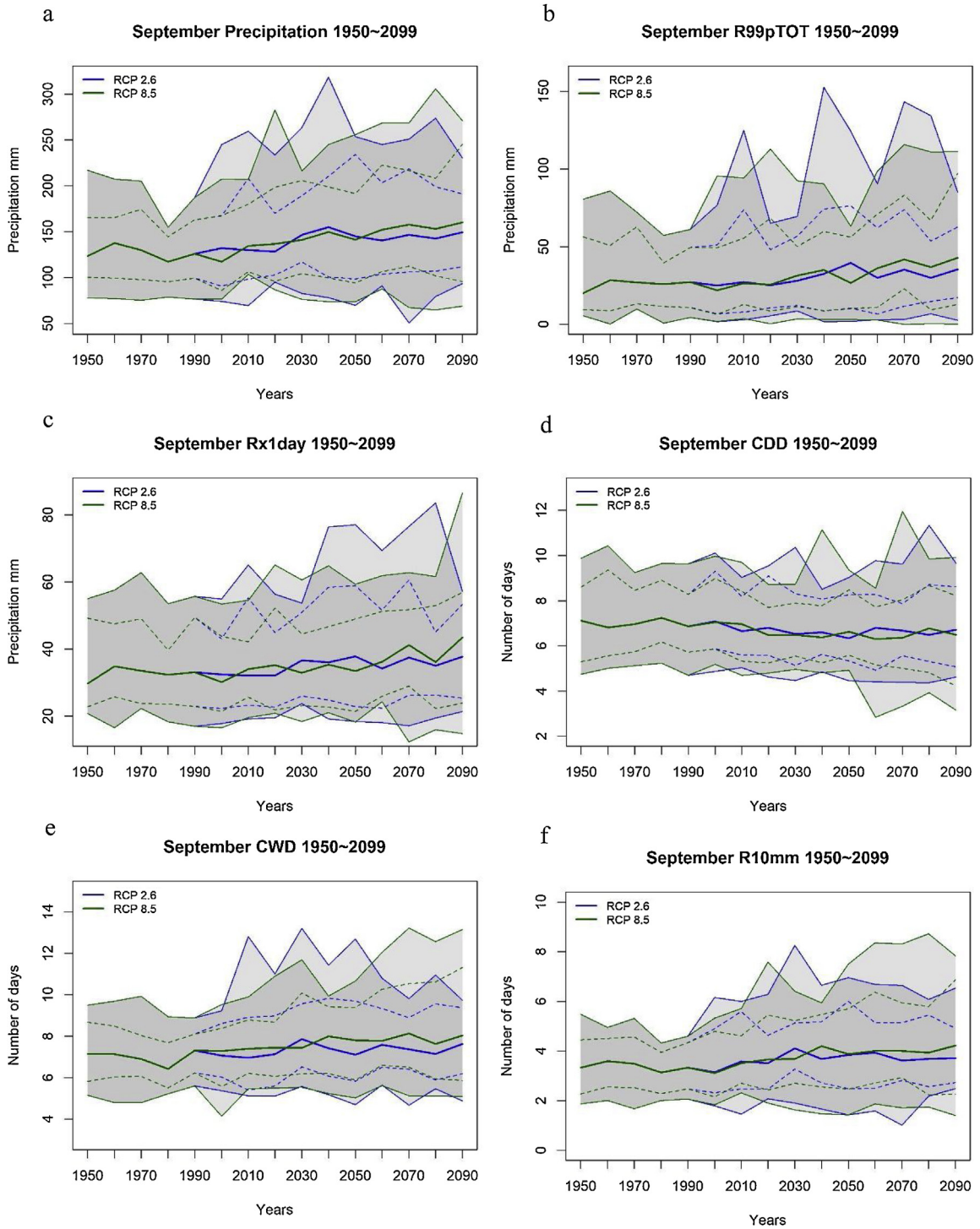

Fig. 7. Same as Fig. 3, but for indices in September from 1950 to 2099.

For example, R10 exhibits a decrease of -0.3 days (-0.8%) for RCP2.6 and -1.0 days (-2.8%) for RCP8.5 in 2010–2039 with respect to the baseline period 1950–1999 (Table 4; Fig. 4). Therefore, the selection of a concentration pathway has little influence on the near-term changes in R10. However, in 2070–2099 the directions of changes are not the same. R10 will increase slightly by 0.2 days (0.7%) for RCP2.6, while a strong decrease of 3.7 days (-10.8%) under RCP8.5 will likely occur during the same period with respect to 1950–1999 (Table 4; Fig. 4). There are decreases in R10 for RCP2.6 in the near and mid-century period and increases back to the initial level in the baseline period. Therefore, fluctuations in R10 occur in RCP2.6 from 1950 to 2099, while a steady decrease in R10 occurs in RCP8.5 over the same period. The differences of the R10 between RCP2.6 and RCP8.5 increase from 0.7 days in the near future to 4.0 days in the end-of-century future. Friedman's test shows that there is a statistically significant difference between both R10 under RCP2.6 versus RCP8.5 and in R20 under RCP2.6 versus RCP8.5 (Table 5).

PRCPTOT is another index that shows statistically significant differences between scenarios (Table 5). Under RCP2.6, the median of PRCPTOT will decrease by 1.6 mm (-0.1%) in 2010–2039, increase by 13.6 mm (1.1%) in 2040–2069, and increase by 11.1 mm (0.9%) in

Table 5
Results of Friedman's test of differences comparing the RCP2.6 and RCP8.5 scenarios 1950-2099. The table shows the p-values. Those that are statistically significant at 0.05 level (*) and at the .01 level (**) are indicated.

Indices	Jan	Feb	Mar	Apr	May	Jun	Jul	Aug	Sep	Oct	Nov	Dec	Annual
Precipitation	0.06	0.53	0.53	0.06	0.06	0.01*	0.21	0.06	0.53	0.06	0.53	0.21	0.01*
PRCPTOT	0.06	0.53	0.53	0.06	0.06	0.01*	0.21	0.06	0.53	0.06	0.53	0.21	0.01*
R95pTOT	0.53	0.53	0.06	0.06	0.06	0.53	0.06	0.21	1	0.21	0.53	0.53	0.06
R99pTOT	1	1	0.53	0.53	0.21	1	0.06	0.01*	0.21	0.21	0.01*	1	0.53
Rx1day	1	0.21	0.21	0.53	0.00**	0.06	0.21	0.53	0.53	0.06	1	0.53	0.21
Rx5day	0.53	0.53	0.21	0.01*	0.01*	0.06	0.21	0.21	0.53	1	1	0.21	0.21
SDII	1	0.53	0.53	1	0.06	0.21	0.06	0.21	0.53	0.53	0.53	0.53	0.06
CDD	0.21	1	0.21	0.01*	0.06	0.01*	0.06	0.21	0.21	1	0.53	0.21	0.21
CWD	0.00**	0.00**	0.01*	0.06	0.53	0.06	0.06	0.01*	0.01*	0.53	0.06	0.01*	0.06
R10	0.06	1	0.21	0.06	0.06	0.01*	0.21	0.21	0.21	0.53	0.06	0.06	0.01*
R20	0.53	0.21	0.21	0.21	0.21	0.06	0.06	0.01*	0.53	0.53	0.53	0.21	0.01*

* Significant at .05 level.
** Significant at .01 level.

2070–2099. The median of PRCPTOT under RCP8.5, however, will decrease by −12.4 mm (−1.0%), −43.3 mm (−3.6%), and −95.2 mm (−7.9%) for the three future periods (Table 4; Fig. 4). The differences between scenarios increase from 10.8 mm in the near future to 106.4 mm at the end-of-century future.

At monthly scale, precipitation amount and frequency also show increasing differences between scenarios towards the end of century. The change directions are different even in the near future for some months. For example, precipitation in June will decrease by −3.8 mm (−3.0%) for RCP2.6, but increase by 1.5 mm (1.2%) for RCP8.5 in 2010–2039. In 2040–2069, precipitation in June will increase by 0.4 mm (0.3%) for RCP2.6 and will decrease by −6.7 mm (−5.4%) for RCP8.5. In 2070–2099, a median decrease of −3.6 mm (−2.9%) will likely occur for RCP2.6, while a decrease of -11.6 mm (-9.3%) will likely occur for RCP8.5 (Fig. 6). The differences of changes between RCP2.6 and RCP8.5 increase from 5.3 mm in the near future to 8.0 mm in the end-of-century future and these differences between scenarios are statistically significant (Table 5).

Precipitation intensity and consecutive wet days have larger changes in RCP2.6 than RCP8.5. For example, R95pTOT will increase by 3.7 mm in mid-of-century and decrease by 1.0 mm at the end-of-century under RCP8.5; however, R95pTOT will increase by 23.8 mm and 22.3 mm in corresponding periods under RCP2.6 (Table 4). Consecutive wet days (CWD) will increase by 0.23 days in the mid-of-century and by 0.03 days in the end-of-century under RCP8.5; however, CWD will have an increase of 0.36 days and 0.25 days in corresponding periods under RCP2.6 (Table 4).

Inter-annual variations in precipitation in RCP8.5 during the last 50 years of the 21 st century (2050–2099) are larger than the inter-annual variations during the baseline period (1950–1999), as indicated by the larger standard deviation (standard deviation is + 5.7 mm for annual precipitation and up to +0.4 days for the duration and frequency indices). On the contrary, RCP2.6 has less inter-annual variations in precipitation in 2050–2099 compared with 1950–1999. The standard deviation decreases by up to −16.8 mm for annual precipitation and by up to −0.4 days for the duration and frequency indices. Therefore, RCP8.5 is associated with a much more variable and extreme precipitation regime, than RCP2.6. This has significant implications since it represents the worst-case scenario for the Clear Creek watershed in terms of hydroclimatic extremes.

In summary, the magnitude and direction of changes in the precipitation indices vary by scenario. Precipitation frequency and amount significantly differ between the two scenarios, and the differences are more pronounced towards the end of century. Changes in precipitation intensity and duration of wet days are larger under RCP2.6 than under RCP8.5, while RCP8.5 has stronger inter-annual changes than RCP2.6.

4. Discussion

4.1. Comparison with previous studies

The findings that precipitation intensity will likely increase significantly, are consistent with previous research. Tebaldi et al. (2006), for example, found that different GCMs consistently simulated greater global precipitation intensity, regardless of the index used. Sun et al. (2007) found that A2 and B1 scenarios showed decreased precipitation frequency and increased precipitation intensity in most GCMs. The changes simulated in precipitation frequency and precipitation intensity were most pronounced for the most extreme precipitation. Zarekarizi et al. (2016) evaluated the Pacific Northwest region of the United States and found that all indices indicated increases in precipitation extremes and, similar to this study, found the greatest increases towards the end of century.

The causal mechanisms that are responsible for the increase in extreme precipitation in this study are likely due to global processes that have been described in previous studies. Trenberth et al. (2003) noted that climate change causes latent heat releases to increase and, through feedbacks, these initial changes are further enhanced through moisture convergence. This ultimately leads to fewer, but more intense precipitation events. The region where Texas is located will be influenced by the poleward expansion of subtropical high-pressure systems and this leads to decreased precipitation on the poleward side of these systems (Trenberth, 2011). Trenberth (2011) concluded that even as the potential for more extreme precipitation occurs from increased concentration of atmospheric water vapor, the number of dry days also increases. This certainly agrees with the projections for the Clear Creek watershed. Allan and Soden (2008) found that observations show even larger increases in precipitation extremes than model simulation. This suggests that the model predictions reported in this paper may under-estimate the future intensification of the hydrological cycle. Loriaux et al. (2016) suggested that heavy precipitation events may correlate with warmer temperature and moister conditions under stronger large-scale convergence. The costal conditions and rising temperature in the Clear Creek watershed may help to explain the projected increases in the number of extreme precipitation events.

Another finding that emerged from this study and agrees with prior research, is that total precipitation will likely decrease and that the dry spells duration will likely increase. Keim et al. (2011), for example, found that most GCMs projected decreases in annual rainfall in the U.S. Gulf Coast despite some model-to-model differences. Djebou and Singh (2016) also found a significant decrease in mean precipitation during spring and summer in the

Texas gulf coast. Global studies that have examined patterns in Texas have also come to similar conclusions (Dai, 2011; Kundzewicz et al., 2014).

The changing patterns of monthly precipitation agree with the dry gets drier, wet gets wetter (DDWW) paradigm. Compared with baseline period, precipitation in the wettest month September also has the largest increasing magnitude in most periods for RCP2.6 and RCP8.5 (Fig. 6). The months that have greatest decrease are usually November for RCP2.6 and April for RCP8.5 (Fig. 6). The driest month (March) also decreases to some extent in most future periods, especially for RCP8.5. This conforms to the DDWW paradigm that is supported by many climate change studies (Chou et al., 2009; Liu and Allan, 2013; Trenberth, 2011).

4.2. Limitations

It is important to note a number of limitations and assumptions of this study. First, this study assumes that the BCSD downscaling is suitable for the study region and that the downscaled data can reliably represent precipitation patterns at the watershed scale. The assumption is based on previous studies that have showed the BCSD data have reasonable accuracy and therefore it has been used in other hydrological analyses of climate change impacts (Chen et al., 2017; Hernandez and Uddameri, 2014; Wood et al., 2004). No downscaling method, however, is perfect and it is possible that using a different downscaling technique may influence the precipitation indices. As noted above, findings from this study are similar to those of previous studies and therefore the impact of adopting a different downscaling approach will be minimal.

Second, given the size of the study watershed, we have chosen to represent the entire watershed using a single set of precipitation indices without examining intra-watershed variations in precipitation patterns. Prior to merging the downscaled GCM data, we compared the precipitation indices across the watershed and found that they were quite consistent. This spatial consistency reduces the sensitivity to different areal weighting methods. For example, the difference between using the arithmetic areal mean annual precipitation (unweighted average of all the grid cells in the watershed) and area-weighted mean annual precipitation for the Clear Creek watershed is only 1.2 mm during the baseline period. There are likely, however, some sub-grid-scale spatial variations in precipitation characteristics that we were not able to capture in this study.

Third, the analysis in this study is based on the multi-model ensemble. One needs to be cautious about interpreting the changes of multi-model median, as the performance of any single model may not be consistent with the ensemble median. A majority of (>18) the GCMs, however, agree on the direction of change. As for agreement on the magnitude, the smallest ranges occur in the 1960s, while the largest ranges mostly occur in the 2050s for RCP2.6 and the 2080s for RCP8.5. The climate models under RCP8.5 have more discrepancy in the predicted changes than under RCP2.6. Due to the dependence of magnitude of changes on the strength of the forcing and the time period (Rajczak and Schär, 2017), the stronger greenhouse gas forcing in RCP8.5 leads to more vigorous changes in precipitation patterns. Not surprisingly, the largest uncertainties tend to occur at the end of the century.

The ensemble median in this study under-estimates the inter-annual variability. This agrees with Cavazos and Arriaga-Ramírez (2012). Similarly, Rupp et al. (2013) evaluated CMIP5 simulations against gridded observed data, including PRISM, and found that nearly all models under-represented the temporal variability of precipitation at annual and 8-year scale. It is worth noting that the focus of this study is not to select a best model or to examine inter-annual variability, but to quantify potential changes in precipitation using the multi-model ensemble.

Finally, TC precipitation is an important cause of extreme rainfall and flooding in this basin (Zhu et al., 2013) and tropical cyclones are likely to become more intense in the future (IPCC, 2007). Due to the resolution of GCMs and the parametrization schemes that they use to represent convection, the GCMs, however, are not able to reliably simulate TCs and TC precipitation (Emanuel et al., 2008; Strazzo et al., 2013). Some recent studies have used novel approaches to predict future changes in TC precipitation (Emanuel, 2017; Zhu et al., 2013). A limitation of this study is that TC precipitation may not be fully represented. Future studies should utilize approaches that can capture how this component will affect precipitation.

4.3. Water resource management implications

Results of this study demonstrate that precipitation in the Clear Creek watershed will occur in fewer, but larger, events and that periods with little-to-no rain will lengthen. This indicates that this watershed will likely be faced with simultaneous increases in flooding and drought risk in the future. The low-lying topography of Houston also increases the susceptibility to flooding and may further exacerbates these risks. Additionally, the population of Houston will likely increase to 3.6 million people by 2060. Therefore, it is crucial that water resource management adapts to these projected climate changes to sustain the increasing population in this highly urbanized watershed.

Reliability, resiliency, and vulnerability are three factors used to evaluate a water resources system (Mujumdar, 2011). As with longer dry spells, it is important to increase the reliability in matching water demand to water supply to sustain a larger population. Possible water management options may include reducing water consumption, increasing the efficiency wastewater recycling, and redesigning reservoir storage to account for the projected reductions in overall precipitation/water supply. Advanced water management models, such as the Water Rights Analysis Package (WRAP) developed in Texas (Wurbs, 2015), can also be applied to understand and improve the reliability of water supply.

Resiliency measures the ability of a water system to recover from shocks, stresses, and failures. The resiliency of a water system can be enhanced by redesigned water-related infrastructure to account for the increasing probability of extreme rainfall events. Redesigning the system, however, is expensive and therefore it calls for a thorough assessment of risk and a cost benefit analysis.

Vulnerability measures the potential damage and exposure of the water system to extreme events. Past studies, such as Zambrano et al. (2017), provide examples of evaluation and quantification of the vulnerability of the water management system. The vulnerability assessment can be used to identify adaptation and mitigation activities. Possible adaptive measures include earlier and more accurate forecasting/warning systems to allow more time to accommodate the upcoming extreme events. Given the projected changes in precipitation patterns in the study watershed, water management agencies should apply this information to evaluate the reliability, resiliency, and vulnerability of the water resources system and identify viable strategies for ensuring water security.

5. Conclusions

This paper evaluated projected future changes in precipitation patterns in the Clear Creek watershed in Houston, Texas, USA. Climate change will have substantial implications for the Clear Creek watershed because of the combination of urban sprawl, low-lying terrain, and proximity to the Gulf of Mexico, which makes it vulnerable to extreme rainfall events and ensuing flooding. A

multi-model ensemble based on 36 downscaled GCMs was generated from CMIP5 models that were downscaled using the Bias Correction and Spatial Disaggregation (BCSD) method. Two climate scenarios (RCP2.6 and RCP8.5) were examined and ten indices represented projected changes in precipitation characteristics in the Clear Creek watershed.

To answer the stated research questions, this study found that (1) mean annual precipitation will likely decrease significantly based on RCP8.5. Extreme precipitation will likely increase and dry spells will lengthen. Precipitation will likely be significantly more variable at the end-of-century than at present. (2) At the monthly scale, September will likely experience simultaneous increases in precipitation amount, precipitation intensity, precipitation frequency and the wet spells length. In contrast, April, May, August, November, and December will experience decreases in precipitation and increases in dry spell duration. The intra-annual precipitation variability will increase. (3) The model-simulated changes in precipitation are more substantial in RCP8.5 than in RCP2.6 and the differences between the scenarios are most pronounced at the end of century.

Results of this study demonstrate that precipitation in the Clear Creek watershed will be concentrated into fewer, but larger, events and that periods of with little-to-no rain will lengthen. This indicates that this watershed will likely face simultaneous increases in flooding and drought risk in the future. Therefore, the increased risk of hydroclimatic extremes poses significant challenges for managing water resources in the Clear Creek watershed. Water management agencies should apply this information to evaluate the reliability, resiliency, and vulnerability of the water resources system and identify viable strategies for ensuring water security.

Acknowledgements

This research was partially funded by The Institute for Sustainable Communities at Texas A&M University. The authors thank Dr. Phil Berke for his leadership and support.

References

Alexander, L., Zhang, X., Peterson, T., et al., 2006. Global observed changes in daily climate extremes of temperature and precipitation. J. Geophys. Res. Atmos. 111.
Allan, R.P., Soden, B.J., 2008. Atmospheric warming and the amplification of precipitation extremes. Science 321, 1481–1484.
Beniston, M., Stephenson, D.B., Christensen, O.B., et al., 2007. Future extreme events in European climate: an exploration of regional climate model projections. Clim. Change 81, 71–95.
Brody, S.D., Sebastian, A., Blessing, R., et al., 2018. Case study results from southeast Houston, Texas: identifying the impacts of residential location on flood risk and loss. J. Flood Risk Manage. 11, S110–S120.
Cavazos, T., Arriaga-Ramírez, S., 2012. Downscaled climate change scenarios for Baja California and the North American monsoon during the twenty-first century. J. Clim. 25, 5904–5915.
Chang, S.E., McDaniels, T.L., Mikawoz, J., et al., 2007. Infrastructure failure interdependencies in extreme events: power outage consequences in the 1998 Ice Storm. Nat. Hazards 41, 337–358.
Chen, Y., Ale, S., Rajan, N., et al., 2017. Modeling the effects of land use change from cotton (Gossypium hirsutum L.) to perennial bioenergy grasses on watershed hydrology and water quality under changing climate. Agric. Water Manage. 192, 198–208.
Chou, C., Neelin, J.D., Chen, C.-A., et al., 2009. Evaluating the “rich-get-richer” mechanism in tropical precipitation change under global warming. J. Clim. 22, 1982–2005.
Dai, A., 2011. Drought under global warming: a review. Wiley Interdiscip. Rev. Clim. Change 2, 45–65.
Dale, A., Fant, C., Strzepek, K., et al., 2017. Climate model uncertainty in impact assessments for agriculture: a multi-ensemble case study on maize in sub-Saharan Africa. Earth's Future 5, 337–353.
Daly, C., Slater, M.E., Roberti, J.A., et al., 2017. High-resolution precipitation mapping in a mountainous watershed: ground truth for evaluating uncertainty in a national precipitation dataset. Int. J. Climatol. 37, 124–137.
Djebou, D.C.S., Singh, V.P., 2016. Impact of climate change on precipitation patterns: a comparative approach. Int. J. Climatol. 36, 3588–3606.
Easterling, D.R., Meehl, G.A., Parmesan, C., et al., 2000. Climate extremes: observations, modeling, and impacts. Science 289, 2068–2074.
Emanuel, K., 2017. Assessing the present and future probability of Hurricane Harvey's rainfall. PNAS 2017, 16222.
Emanuel, K., Sundararajan, R., Williams, J., 2008. Hurricanes and global warming: results from downscaling IPCC AR4 simulations. Bull. Am. Meteorol. Soc. 89, 347–368.
Fowler, H., Kilsby, C., 2003. Implications of changes in seasonal and annual extreme rainfall. Geophys. Res. Lett. 30.
Gao, X., Shi, Y., Song, R., et al., 2008. Reduction of future monsoon precipitation over China: comparison between a high resolution RCM simulation and the driving GCM. Meteorol. Atmos. Phys. 100, 73–86.
Gharbia, S.S., Gill, L., Johnston, P., et al., 2016. Multi-GCM ensembles performance for climate projection on a GIS platform. Model. Earth Syst. Environ. 2, 102.
Grant, N., Saito, L., Weltz, M., et al., 2013. Instrumenting wildlife water developments to collect hydrometeorological data in remote western US catchments. J. Atmos. Oceanic Technol. 30, 1161–1170.
Hagedorn, R., DOBLAS-REYES, F.J., Palmer, T., 2005. The rationale behind the success of multi-model ensembles in seasonal forecasting–I. Basic concept. Tellus A 57, 219–233.
Hernandez, E.A., Uddameri, V., 2014. Standardized precipitation evaporation index (SPEI)-based drought assessment in semi-arid south Texas. Environ. Earth Sci. 71, 2491–2501.
Hollander, M., Wolfe, D.A., Chicken, E., 2013. Nonparametric Statistical Methods, Vol. 751. John Wiley & Sons.
IPCC, 2007. Climate change 2007: the physical science basis. Contribution of Working Group I to the Fourth Assessment Report of the Intergovernmental Panel on Climate Change, .
IPCC, 2013. Climate change 2013: the physical science basis. Contribution of Working Group I to the Fifth Assessment Report of the Intergovernmental Panel on Climate Change. Cambridge University Press.
Keim, B.D., Fontenot, R., Tebaldi, C., et al., 2011. Hydroclimatology of the US Gulf Coast under global climate change scenarios. Phys. Geogr. 32, 561–582.
Kundzewicz, Z.W., Kanae, S., Seneviratne, S.I., et al., 2014. Flood risk and climate change: global and regional perspectives. Hydrol. Sci. J. 59, 1–28.
Kunkel, K.E., 2003. North American trends in extreme precipitation. Nat. Hazards 29, 291–305.
Liu, C., Allan, R.P., 2013. Observed and simulated precipitation responses in wet and dry regions 1850–2100. Environ. Res. Lett. 8, 034002.
Loriaux, J.M., Lenderink, G., Siebesma, A.P., 2016. Peak precipitation intensity in relation to atmospheric conditions and large-scale forcing at midlatitudes. J. Geophys. Res. Atmos. 121, 5471–5487.
McSweeney, C.F., Jones, R.G., 2016. How representative is the spread of climate projections from the 5 CMIP5 GCMs used in ISI-MIP? Climate Serv. 1, 24–29.
Mujumdar, P., 2011. Implications of Climate Change for Water Resources Management. India Infrastructure Report, 18. .
PRISM Climate Group, Oregon State University, http://prism.oregonstate.edu, created 18 August 2014.
Rajczak, J., Schär, C., 2017. Projections of future precipitation extremes over Europe: a multimodel assessment of climate simulations. J. Geophys. Res. Atmos. 122.
Rosenzweig, C., Tubiello, F.N., Goldberg, R., et al., 2002. Increased crop damage in the US from excess precipitation under climate change. Global Environ. Change 12, 197–202.
Rupp, D.E., Abatzoglou, J.T., Hegewisch, K.C., et al., 2013. Evaluation of CMIP5 20th century climate simulations for the Pacific Northwest USA. J. Geophys. Res. Atmos. 118 (10) 884-810,906.
Shields, C.A., Kiehl, J.T., Meehl, G.A., 2016. Future changes in regional precipitation simulated by a half-degree coupled climate model: sensitivity to horizontal resolution. J. Adv. Model. Earth Syst. 8, 863–884.
Shrestha, A.B., Bajracharya, S.R., Sharma, A.R., et al., 2017. Observed trends and changes in daily temperature and precipitation extremes over the Koshi river basin 1975–2010. Int. J. Climatol. 37, 1066–1083.
Strachan, S., Daly, C., 2017. Testing the daily PRISM air temperature model on semiarid mountain slopes. J. Geophys. Res. Atmos. 122, 5697–5715.
Strazzo, S., Elsner, J.B., LaRow, T., et al., 2013. Observed versus GCM-generated local tropical cyclone frequency: comparisons using a spatial lattice. J. Clim. 26, 8257–8268.
Sun, Y., Solomon, S., Dai, A., et al., 2007. How often will it rain? J. Clim. 20, 4801–4818.
Tebaldi, C., Hayhoe, K., Arblaster, J.M., et al., 2006. Going to the extremes. Clim. Change 79, 185–211.
Trenberth, K.E., 2011. Changes in precipitation with climate change. Clim. Res. 47, 123–138.
Trenberth, K.E., Dai, A., Rasmussen, R.M., et al., 2003. The changing character of precipitation. Bull. Am. Meteorol. Soc. 84, 1205–1218.
US Census, 2017. US Census, United States Census Bureau, 2017 URL. . https://www.census.gov/quickfacts/fact/table/houstoncitytexas,US/PST045217#viewtop.
van Oldenborgh, G.J., van der Wiel, K., Sebastian, A., et al., 2017. Attribution of extreme rainfall from Hurricane Harvey, August 2017. Environ. Res. Lett. 12, 124009.
Wasko, C., Sharma, A., 2017. Global assessment of flood and storm extremes with increased temperatures. Sci. Rep. 7, 7945.
Weigel, A.P., Liniger, M., Appenzeller, C., 2008. Can multi-model combination really enhance the prediction skill of probabilistic ensemble forecasts? Q. J. R. Meteorolog. Soc. 134, 241–260.

Westra, S., Fowler, H., Evans, J., et al., 2014. Future changes to the intensity and frequency of short-duration extreme rainfall. Rev. Geophys. 52, 522–555.
Woldemeskel, F.M., Sharma, A., Sivakumar, B., et al., 2012. An error estimation method for precipitation and temperature projections for future climates. J. Geophys. Res. Atmos. 117.
Wood, A.W., Leung, L.R., Sridhar, V., et al., 2004. Hydrologic implications of dynamical and statistical approaches to downscaling climate model outputs. Clim. Change 62, 189–216.
Wurbs, R.A., 2015. Institutional and hydrologic water availability in Texas. Water Resour. Manage 29, 217–231.
Zambrano, L., Pacheco-Muñoz, R., Fernández, T., 2017. A spatial model for evaluating the vulnerability of water management in Mexico City, Sao Paulo and Buenos Aires considering climate change. Anthropocene 17, 1–12.
Zarekarizi, M., Rana, A., Moradkhani, H., 2016. Precipitation extremes and their relation to climatic indices in the Pacific Northwest USA. Clim. Dyn. 1–19.
Zhu, L., Quiring, S.M., Emanuel, K.A., 2013. Estimating tropical cyclone precipitation risk in Texas. Geophys. Res. Lett. 40, 6225–6230.
Zhu, L., Quiring, S.M., Guneralp, I., et al., 2015. Variations in tropical cyclone-related discharge in four watersheds near Houston. Texas. Clim. Risk Manage. 7, 1–10.